Journal of Systems Engineering and Electronics
Vol. 28, No. 3, June 2017, pp.424 – 434

Schemes for synthesizing high-resolution range profile with extended OFDM-MIMO

Xinhai Wang[1,2], Gong Zhang[1,2,*], Fangqing Wen[3], and De Ben[1,2]

1. Key Laboratory of Radar Imaging and Microwave Photonics, Nanjing University of Aeronautics and Astronautics, Nanjing 211106, China;
2. College of Electronic and Information Engineering, Nanjing University of Aeronautics and Astronautics, Nanjing 211106, China;
3. Electronic and Information School, Yangtze University, Jingzhou 434023, China

Abstract: Two novel schemes are proposed to synthesize high-resolution range profile (HRRP) based on co-located multiple-input multiple-output (MIMO) system in the context of the joint radar and communication system. The difference between two schemes is the pattern of selecting pulses, which depends on the demand for the velocity information. The system, a type of frequency diverse array (FDA), takes full advantage of the phase-coded orthogonal frequency division multiplexing (OFDM) signal. Furthermore, the complete discrete form of the phase-coded OFDM echoes is utilized to derive the HRRP processing. The velocity estimation in the second scheme aims to eliminate velocity ambiguity, and high velocity can be retrieved exactly. Meanwhile, the imaging method is investigated with random frequency coding applied to an array. The desired performance of resolving velocity ambiguity and suppressing noise is shown by means of comparisons with previous work. The advantages in the radar imaging and the significance of the work are concluded in the end.

Keywords: high-resolution range profile (HRRP), multiple-input multiple-output system (MIMO), orthogonal frequency division multiplexing (OFDM), joint radar-communication system.

DOI: 10.21629/JSEE.2017.03.02

1. Introduction

The idea of combining a radar and a communication system on the same platform was studied in [1]. Incipiently the most evident hurdle is that radars and communication systems are separated because of different frequency ranges. With the development of the radio frequency front-end systems, the differences between hardware requirements for the radar and communication systems are diminishing. Simultaneously the orthogonal frequency division multiplexing (OFDM) signal becomes the most popular choice in the area where the radar and communication functionalities are combined [2].

High-resolution range profile (HRRP) can be obtained by using a waveform with large enough time-bandwidth products, which is widely applied in the fields of target recognition and air traffic control, etc. [3]. However, the generation of the signal with large time-bandwidth products is difficult for hardware implementation. To improve the total bandwidth and range resolution, a stepped-frequency mode was implemented by maintaining a fixed frequency spacing of 100 MHz in a burst in [4], and the instantaneous bandwidth and required sampling rate are limited. Some methods using several pulses to synthesize a chirp with large bandwidth were known as stepped-frequency chirp and frequency-jumped burst in [5]. Based on the above work, a method which achieves large bandwidth with a synthetic chirp waveform adequate for short transmitted pulses was presented in [6]. The instantaneous wideband waveform can be also synthesized by developing the potential advantages of the multiple-input multiple-output (MIMO) systems based on frequency diversity. In this regard, a novel system, OFDM-MIMO phased radar system, was proposed to improve the detection performance of a high speed moving target in [7,8], which also weakens the effect of the high velocity, reaping the benefit of the parallel incoherent processing of the spatial diversity multi-channel data in a short time. And the individual phased array element transmits chirp signals modulated by a carrier frequency equivalent to one of the subcarriers in an OFDM symbol. A scheme of a large time-bandwidth product waveform diversity based on

Manuscript received August 18, 2016.
*Corresponding author.
This work was supported by the National Natural Science Foundation of China (61071163; 61071164; 61471191; 61501233), the Fundamental Research Funds for the Central Universities (NP2014504), the Aeronautical Science Foundation (20152052026), the Electronic & Information School of Yangtze University Innovation Foundation (2016-DXCX-05), the Funding for Outstanding Doctoral Dissertation in NUAA (BCXJ15-03), the Funding of Jiangsu Innovation Program for Graduate Education (KYLX15 0281), the Fundamental Research Funds for the Central Universities and partly funded by the Priority Academic Program Development of Jiangsu Higher Education Institutions (PADA).

chirp rate diversity has been put forward for MIMO radar in [9]. However, the chirp signal has the disadvantage of range-Doppler coupling inherently and its applications in the communication systems are fewer than those of OFDM signals.

Compared with chirp signals, the OFDM waveform has shown its superiority in terms of the spectrum efficiency, the scalability of bandwidth, transmission rate and the capability of anti-multipath [10,11]. Overall, the OFDM signal is highly appropriate in applications which radar and communication joint functionalities are available for. In [12], a technique which exploits the multicarrier structure of OFDM waveform and the random phase modulation on the carriers was suggested to estimate the range and Doppler of a moving target unambiguously. In another paper [13], a range-Doppler estimation scheme for continuous OFDM signals is proposed for automotive applications. One of their common characteristics is that the above schemes are performed under the background of single-input and single-output (SISO) radar systems, another is the form of the OFDM pulse which combines intra-pulse frequency weighting and complementary coding sequences. The quantity of literature available concerned with the OFDM pulsed radar is not large.

As a result of the complex electromagnetic environment and the development of electronic countermeasure technology, the phase-coded OFDM waveform has attracted the attention of researchers as a result of its outstanding anti-jamming potential, simple realization and their inheritance of low-probability of intercept (LPI) performance from OFDM signals. A novel signal processing scheme was examined in [14], which achieves the estimation of range and radial velocity based on phase-coded OFDM signals. According to this idea, a new signal structure, frequency-agile phase-coded OFDM waveform, which enables the Doppler to be solved in spite of the existence of frequency agility was proposed in [15]. Thus, the wideband is synthesized by a few pulses with different carrier frequencies. Benefitting from the aforementioned signal structure, HRRP is synthesized in slow time after a matched filter is applied to the individual pulse in [16]. The pulse compression provides a coarse range resolution determined by the bandwidth of single OFDM pulses. However, the influence of Doppler shift was not taken into consideration. Since then, in [17] and [18], the ambiguity function of phase-coded OFDM signals and the expression of HRRP were analyzed, presenting the influence of the target velocity and investigating the parameterization and the velocity compensation. Nevertheless, the anti-jamming capability is not strong enough in comparison with the approach mentioned as follows. A new framework for the OFDM phase-coded stepped-frequency waveform based on the inter-pulse Costas frequency coding was developed to produce HRRP in [19]. However, there is no comparison between the proposed method and other available schemes, and its scheme is only based on Costas frequency coding without universal explanation. One of the most obvious flaws is that the wideband OFDM phase-coded stepped-frequency waveform is difficult to be generated for the hardware. Another is that the communication speed is restricted in the SISO system.

MIMO is usually utilized in wireless communication and radio frequency detection. The combination of co-located MIMO radar and the structural sparsity Bayesian learning was used in direction-of-arrival (DOA) estimation in [20]. Under the background of the MIMO radar with arbitrary array shape, the multi-compressive sensing achieved the 2-dimension DOA estimation in [21]. Detection is one of the most important abilities for radar systems. The concept of MIMO high-resolution radar system is derived from the fact that the MIMO is introduced to achieve the detection and imaging of moving targets. For moving targets, not only can the long-time integration be avoided, but also the velocity compensation processing may be left out. An arrangement mode of array elements was presented for MIMO radar imaging of airborne moving targets in [22]. Then a lot of research achievements have been made recently. Some approaches of high-resolution imaging based on co-located and distributed MIMO systems were proposed in [23] and [24] respectively. Meanwhile, a method of imaging with the high azimuth resolution using the MIMO radar array was given by analyzing the spatial spectral domain in [25]. The transmitted signal of each element in the MIMO systems mentioned above is a waveform with arbitrary single frequency. As a result, the different carriers and sidebands may interfere with each other and the spectrum utilization may be inefficient. A scheme of using a reciprocal spectrum filter to suppress the high-level sidelobes near and far from the mainlobe and the interferences between the harmonic components was proposed in [26]. However, the problem can be solved by OFDM technique easily, and the spectrum efficiency is able to be increased to a large extent. With the development of the OFDM radar [27], the imaging method based on the OFDM-MIMO system was presented in [28]. The OFDM signal provides superior control over the spectrum because the modulation technique dominates the amplitude and the initial phase of each harmonic component which composes the signal. And a new waveform, the orthogonal frequency division linear frequency modulation (OFD-LFM) signal, is the combination of the OFDM technology and the linear frequency modulated (LFM) signal [29]. The OFD-LFM applied in MIMO radar imaging possesses good orthogonality, the large synthetic bandwidth and the insensitivity to velocity [30,31]. However the LFM signal has the problem of range-Doppler coupling.

Considering the aforementioned drawbacks of existing work, we propose two schemes based on the MIMO system to obtain the HRRP of a moving target. The velocity estimation can be conducted without velocity ambiguity. The performance of suppressing noise is also discussed in simulation experiments. Meanwhile, the range extent of the proposed schemes will be larger than that of the OFD-LFM system if both systems are performed using the exactly similar parameters. Furthermore, our work conforms to the development tendency of the joint radar and communication system.

2. Synthesizing HRRP with extended OFDM-MIMO

2.1 Model of radar system

In MIMO system, each receiving antenna may accept the signal transmitted by every array element. Therefore, all the transmitted signals should be orthogonal to each other to tell each signal apart from the echoes in reception. Generally, the carrier frequencies are equally spaced by the frequency spacing. The pattern is called frequency diverse array (FDA). As shown in Fig. 1(a), R_0 is the distance between the reference element and the target with d denoting the element spacing. Then $R_0 + (m-1)d\sin\theta$ is the slant range for the mth element. The FDA looks like an OFDM-MIMO radar mentioned in [32] where the OFDM signal has been transmitted by the antenna array. And Fig. 1(b) illustrates the relation between the array elements mentioned in Fig. 1(a) and the spectra of their transmitted waveforms. Assume that the variables $f_1, f_2, \dots, f_M$ are the center frequencies of the radio-frequency signal transmitted by the corresponding elements, and the bandwidth of the narrowband signal B_s is equal to the frequency spacing of the carriers. The transmitted signal of each element can be extended to the phase-coded OFDM waveform. Therefore, the system is called extended OFDM-MIMO in this paper.

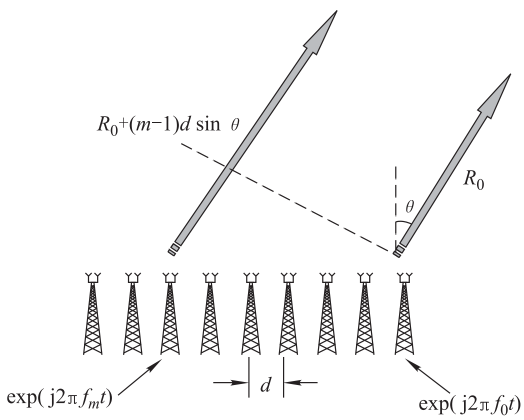

(a) Sketch of standard FDA

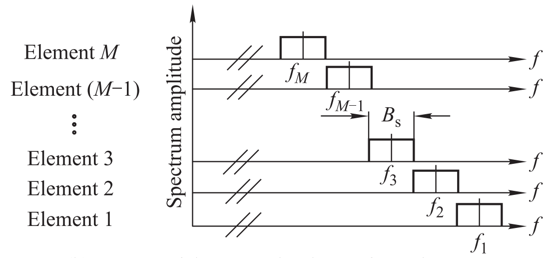

(b) Spectra of the transmitted waveforms in FDA

Fig. 1 Signal model of FDA

For convenience, the co-located MIMO is taken as an example in this paper, and the signal pattern refers to the FDA shown in Fig. 1(b) similar to OFDM-MIMO. Two schemes based on the pattern described above are able to resist the influence of velocity. Both proposed schemes are shown in Fig. 2. In detail, Scheme I in Fig. 2(a) may be performed to image in the case that the velocity estimation is not required since the echoes come from the pulses transmitted by all array elements simultaneously. On the contrary, Scheme II in Fig. 2(b) is capable of realizing the estimation of range and radial velocity simultaneously because the echoes are received from pulses with different emission time. It is worth mentioning that the beam forming technique makes the signal transmitted and received by the reference element equivalently. Therefore, the following analyses are supposed to be performed after the beam forming processing. The carrier frequencies of all elements are described in Fig. 2(c). The order of their frequencies is determined by the sequence of frequency codes.

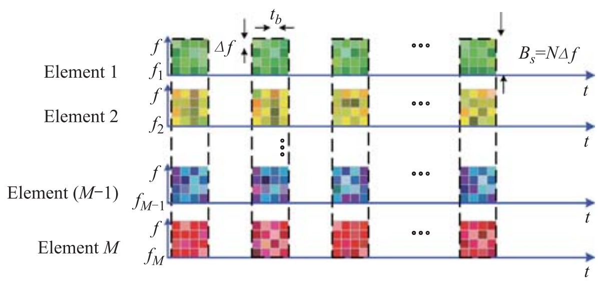

(a) Selection of the transmitted pulses of Scheme I

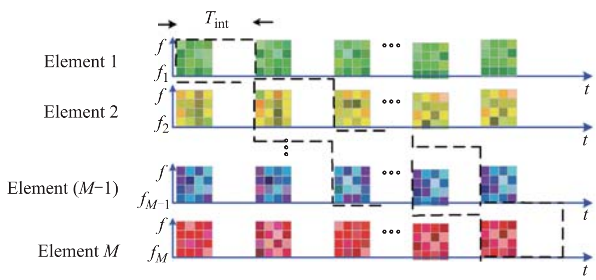

(b) Selection of the transmitted pulses of Scheme II

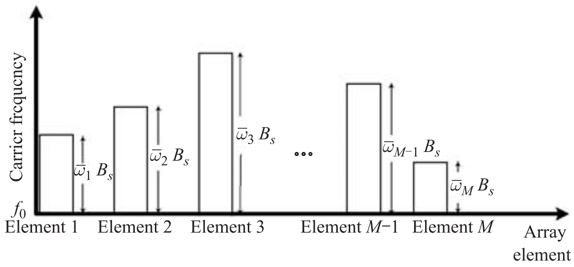

(c) Carrier frequency of each element

Fig. 2 Signal model of the proposed OFDM-MIMO

2.2 Transmitted signal

Assume that the array manifold complies by the uniform linear array with M array elements. The phase-coded OFDM complex envelope of the mth element can be expressed as

$$u_m(t) = A_m \sum_{n=0}^{N-1} \sum_{k=0}^{K-1} \omega_n a_{k,n,m} \mathrm{rect}\left[\frac{t - t_b/2 - kt_b}{t_b}\right] \cdot \exp(\mathrm{j}2\pi n\Delta f t) \tag{1}$$

where N is the number of subcarriers, K is the number of chips, ω_n is the complex modulation coefficient of the nth subcarrier and t_b is the duration of a chip. And $a_{k,n,m}$ is the phase code of the kth chip, the nth subcarrier and the transmitted waveform of the mth element. The subcarrier spacing denoted by Δf is equal to $1/t_b$. $\mathrm{rect}\left(\dfrac{t}{T}\right) = \begin{cases} 1, & -T/2 \leqslant t \leqslant T/2 \\ 0, & \text{otherwise} \end{cases}$. And the bandwidth of a single pulse $B_s = N\Delta f$ is equal to the frequency spacing of the carrier frequencies. The symbol A_m is introduced to normalize the power of a single pulse. Then the expression for the transmitted pulse of the mth element is given as

$$s_{t,m}(t) = u_m(t - iT_{\mathrm{int}}) \exp(\mathrm{j}2\pi f_m t), \quad i = 0, 1, 2, \ldots \tag{2}$$

where the expression $u_m(t - iT_{\mathrm{int}})$ denotes the $(i+1)$th phase-coded OFDM pulse whose pulse repetition interval (PRI) is equal to T_{int}. And the variable f_m expressed by $f_m = f_0 + (\boldsymbol{\omega}(m) - 1)B_s$ is the carrier frequency of the mth element and f_0 is the lowest carrier frequency. The vector $\boldsymbol{\omega}$ is a set of carrier frequency codes.

The ambiguity function of phase-coded OFDM signals is depicted in Fig. 3(a). As shown in Fig. 3(b), the cross sections of ambiguity function indicate that the range and velocity resolution of a phase-coded OFDM waveform should be $c/2B_s$ and $1/Kt_b$ respectively, and the symbol c denotes the speed of light.

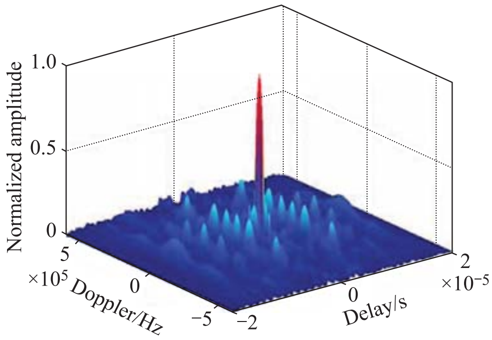

(a) Ambiguity function of a single phase-coded OFDM pulse

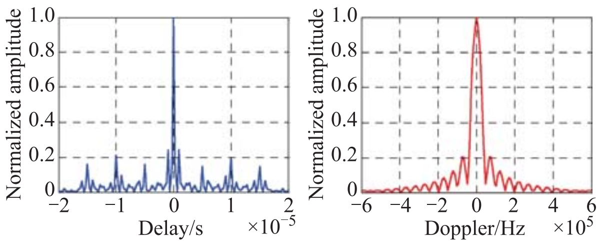

(b) Blue line is the section of the delay and the red one is the section of the Doppler

Fig. 3 Ambiguity function of phase-coded OFDM signal

2.3 Received signal

It is a critical step for the design of processing technique to model the echoes in the receiver. With phase-coded OFDM pulsed radar, the multicarrier nature of the OFDM structure encourages accurate modeling of the range migration because of the sensitivity of the subcarriers with respect to variations in the phase. For co-located extended OFDM-MIMO radar, the selection of pulses may influence the processing approach. Both schemes of selecting the pulses from each transmitting element are illuminated in Fig. 2(a) and Fig. 2(b) respectively. In Scheme I, the echoes of the signal emitted simultaneously are accumulated in the receiving terminal, which can avert the impact of the relative displacement in a coherent processing interval (CPI). Considering the estimation of the radial velocity, Scheme II is supposed to be performed because the velocity information embedded in a group of the selected pulses which come from all elements and are staggered successively in the time domain. For the above two schemes, the echoes of the selected pulses compose the original data utilized for imaging. In addition, the carrier frequency configuration for the proposed OFDM-MIMO is described in Fig. 2(c). Without loss of generality, Scheme II is discussed in this section. The Scheme I can be analyzed analogously.

Assume that the target consists of L scattering centers and the motion of the whole scatter with radial velocity v is described by $R(t) = R_0 + vt$, where R_0 denotes the initial radial distance between the target and the radar. Then the received echo of the signal transmitted by the mth element is given by

$$s_{r,m}(t)=\sum_{l=1}^{L}\rho_l s_{t,m}(t-\tau_{m,l}) \tag{3}$$

where ρ_l is the complex reflectivity coefficient of the lth scattering center. As a matter of convenience, the term $\tau_{m,l}=2(R_{0l}+vt)/c$ stands for the two-way time delay from the reference point of the transmitting array to that of the receiving array, the signal reflecting from the lth scattering point. And R_{0l} denotes the initial distance of the lth scattering point. The expression $\exp(\mathrm{j}2\pi f_m t)$ is used to model the mixing process in the receiver, which is multiplied by the received echo of the signal transmitted by the mth element. The baseband signal of the mth element in reception is expressed as

$$s_{b,m}(t)=\sum_{l=1}^{L}\rho_l\exp(-\mathrm{j}2\pi f_m\tau_{m,l})\cdot$$
$$\exp[\mathrm{j}2\pi f_{Dm,l}t]u_m(t-\tau_{m,l}) \tag{4}$$

where $f_{Dm,n,l}=2v(f_m+n\Delta f)/c$ is the Doppler frequency. In the context of extended OFDM-MIMO, the Doppler shift may differ from one element to another because of the different carrier frequencies.

The discrete form of baseband signals is derived by sampling the signal in the time domain according to Nyquist theorem. The sampling frequency is assumed to be $f_s=N/t_b=N\Delta f$, and the sampling time axis is shown as $(p_0+kt_b+n_t/N\cdot t_b)$, where $n_t=0,1,\ldots,N-1$. Therefore, the discrete form is expressed as

$$s_{m,k,p}(n_t)=$$
$$\sum_{l=1}^{L}\sum_{n=0}^{N-1}\rho_l\omega_n a_{k,n,m}\exp[-\mathrm{j}2\pi(f_m+n\Delta f)\tau_l]\cdot$$
$$\exp\left[\mathrm{j}2\pi n\Delta f\left(p_0+kt_b+\frac{n_t}{N}t_b-\tau_l\right)\right]\cdot$$
$$\exp\left[\mathrm{j}2\pi f_{D_{m,n,l}}\left(p_0+kt_b+\frac{n_t}{N}t_b-\tau_l\right)\right] \tag{5}$$

where

$$n_t=0,1,\ldots,N-1$$
$$p_0=[\lfloor 2R_0f_s/c\rfloor+1]/f_s=qt_b/N$$
$$\tau_{m,l}=2(R_0+mvT_{\mathrm{int}})/c.$$

The operator $\lfloor\cdot\rfloor$ returns the greatest integer equal to or less than its numerical argument, and T_{int} is equal to PRI. An N-element vector which denotes the kth chip of the complex baseband echo made by the mth transmitting element and returning from the lth scattering point is given by

$$\boldsymbol{s}_{\mathrm{d}m,k,l}=\rho_l\alpha_{m,l}\boldsymbol{V}_{m,n,k,l}\boldsymbol{\Lambda}\boldsymbol{\Gamma}_{m,n,k,l}\boldsymbol{D}_{m,k}\boldsymbol{\Omega}. \tag{6}$$

All the terms in (6) can be expressed as follows:

$$\alpha_{m,l}=\exp(-\mathrm{j}2\pi f_m\tau_{m,l}). \tag{7}$$

The matrix $\boldsymbol{V}_{m,n,k,l}$ includes the Doppler shift information as follows:

$$\boldsymbol{V}_{m,n,l}=\exp\left[\mathrm{j}2\pi\frac{2v}{c}f_m(p_0+kt_b-\tau_{m,l})\right]\cdot$$
$$\exp\left(\mathrm{j}2\pi\frac{2v}{c}f_m\frac{n_t}{N}t_b\right)\cdot$$
$$\exp\left[\mathrm{j}2\pi\frac{2v}{c}n\Delta f(p_0+kt_b-\tau_{m,l})\right]\cdot$$
$$\exp\left(\mathrm{j}2\pi\frac{2v}{c}n\Delta f\frac{n_t}{N}t_b\right)=$$
$$\exp\left[\mathrm{j}2\pi\frac{2v}{c}f_m(p_0+kt_b-\tau_{m,l})\right]\boldsymbol{V}_1\boldsymbol{V}_2\boldsymbol{V}_3 \tag{8}$$

$$\boldsymbol{V}_1=\mathrm{diag}(1,v_1,v_1^2,\ldots,v_1^{N-1}) \tag{9}$$
$$v_1=\exp\left(\mathrm{j}2\pi\frac{2v}{c}f_m\frac{t_b}{N}\right)$$

$$\boldsymbol{V}_2=\mathrm{diag}(1,v_2,v_2^2,\ldots,v_2^{N-1}) \tag{10}$$
$$v_2=\exp\left(\mathrm{j}2\pi\frac{2v}{c}\Delta f(p_0+kt_b-\tau_{m,l})\right)$$

$$\boldsymbol{V}_3=\begin{bmatrix}1 & 1 & 1 & \cdots & 1\\ 1 & v_3 & v_3^2 & \cdots & v_3^{N-1}\\ 1 & v_3^2 & v_3^4 & \cdots & v_3^{2(N-1)}\\ \vdots & \vdots & \vdots & \ddots & \vdots\\ 1 & v_3^{N-1} & v_3^{2(N-1)} & \cdots & v_3^{(N-1)^2}\end{bmatrix} \tag{11}$$
$$v_3=\exp\left(\mathrm{j}2\pi\frac{2v}{c}\Delta f\frac{t_b}{N}\right).$$

Note that the operator $\mathrm{diag}(\cdot)$ is a diagonal matrix formed by components of the vector argument in the parentheses. Since the condition of the narrow-band transmitted signal is satisfied, i.e., $f_m\gg N\Delta f$, both terms, V_2 and V_3, can be neglected. The mentioned relationship $t_b\cdot\Delta f=1$ will be immensely helpful to the following analysis. Other variables are given as

$$\boldsymbol{\Lambda}=\begin{bmatrix}1 & 1 & 1 & \cdots & 1\\ 1 & \eta_3 & \eta_3^2 & \cdots & \eta_3^{N-1}\\ 1 & \eta_3^2 & \eta_3^4 & \cdots & \eta_3^{2(N-1)}\\ \vdots & \vdots & \vdots & \ddots & \vdots\\ 1 & \eta_3^{N-1} & \eta_3^{2(N-1)} & \cdots & \eta_3^{(N-1)^2}\end{bmatrix} \tag{12}$$

$$\eta=\exp\left(\mathrm{j}2\pi\Delta f\frac{t_b}{N}\right) \tag{13}$$

$$\boldsymbol{\Gamma}_{m,n,k,l}=\mathrm{diag}(1,\gamma,\gamma^2,\ldots,\gamma^{N-1}) \tag{14}$$

$$\gamma = \exp[\mathrm{j}2\pi\Delta f(p_0 + kt_b - \tau_{m,l})] = \exp[\mathrm{j}2\pi\Delta f(p_0 - \tau_{m,l})] \tag{15}$$

$$\boldsymbol{D}_{k,m} = \mathrm{diag}(a_{0,k,m}, a_{1,k,m}, \ldots, a_{N-1,k,m}) \tag{16}$$

$$\boldsymbol{\Omega}^{\mathrm{T}} = [\omega_0, \omega_1, \ldots, \omega_{N-1}]. \tag{17}$$

The matrix $\boldsymbol{\Lambda}$ happens to be the inverse discrete Fourier transform (IDFT) matrix $\boldsymbol{F}^{-1}$, with the variable η reducing to $\exp(\mathrm{j}2\pi/N)$. The matrix $\boldsymbol{D}_{m,k}$ and the vector $\boldsymbol{\Omega}$ consist of the phase codes of the kth chip and the complex modulation coefficients of the subcarriers respectively. Then the final expression of the chip echo can be expressed by

$$\boldsymbol{s}_{\mathrm{d}m,k,l} = \rho_l \alpha_{m,l} \kappa_{m,l} \boldsymbol{V}_1 \boldsymbol{F}^{-1} \boldsymbol{\Gamma}_{m,n,k,l} \boldsymbol{D}_{m,k} \boldsymbol{\Omega} \tag{18}$$

where $\kappa_{m,l} = \exp[\mathrm{j}4\pi v f_m(p_0 + kt_b - \tau_l)/c]$.

2.4 Signal processing of synthesizing HRRP

After the Doppler compensation, $\boldsymbol{V}_1$ is reduced to an identity matrix $\boldsymbol{I}_N$. Then (11) can be simplified by multiplying both sides with the discrete Fourier transform (DFT) matrix $\boldsymbol{F}$ because of $\boldsymbol{F}\boldsymbol{F}^{-1} = \boldsymbol{I}_N$. The frequency expression of $\boldsymbol{s}_{\mathrm{d}m,k,p}$ is expressed as

$$\boldsymbol{\sigma}_{\mathrm{d}k,m,l} = \rho_l \alpha_{m,l} \kappa_{m,l} \boldsymbol{\Gamma}_{m,n,k,l} \boldsymbol{D}_{m,k} \boldsymbol{\Omega}. \tag{19}$$

The components of $\boldsymbol{\sigma}_{\mathrm{d}m,k,l}$ contain the information of all subcarriers from the current chip, e.g. the weights, phase codes and others caused by the characteristics of targets. Furthermore, the weighted parameters of the subcarriers and the phase codes of the chips carried by the phase-coded OFDM signal are the useful information for communication, but the echoes without them are quite important for the radar signal processing. Hence, we should remove the phase codes and the weighted parameters in order to extract the terms related to the targets. The conjugate phase codes of the K chips in the same pulse can be written in a matrix $\boldsymbol{C}_m$.

$$\boldsymbol{C}_m = \begin{bmatrix} a^*_{0,0,m} & a^*_{0,1,m} & \cdots & a^*_{0,N-1,m} \\ a^*_{1,0,m} & a^*_{1,1,m} & \cdots & a^*_{1,N-1,m} \\ \vdots & \vdots & \ddots & \vdots \\ a^*_{K-1,0,m} & a^*_{K-1,1,m} & \cdots & a^*_{K-1,N-1,m} \end{bmatrix}. \tag{20}$$

The complete data from a pulse of the mth element in the frequency domain can be stacked in a close matrix according to the order of the chips as follows:

$$\boldsymbol{G}_{m,l} = \begin{bmatrix} \boldsymbol{\sigma}_{\mathrm{d}0,m,l} & \boldsymbol{\sigma}_{\mathrm{d}1,m,l} & \cdots & \boldsymbol{\sigma}_{\mathrm{d}K-1,m,l} \end{bmatrix}. \tag{21}$$

The diagonal elements of the matrix $\boldsymbol{G}_{m,l}\boldsymbol{C}_m$ can be extracted to assemble the column vector $\boldsymbol{g}_{m,l}$ which contains the target information and the residual terms produced by weighted parameters and the phase codes. The vector without the residual terms is derived by

$$\boldsymbol{r}_{m,l}(n) = \frac{\boldsymbol{g}_{m,l}(n)}{\omega_n \cdot \boldsymbol{b}_{m,l}(n)} = N\rho_l \alpha_{m,l} \gamma^n. \tag{22}$$

Note that $\boldsymbol{b}_{m,l}(n) = \sum_{k=0}^{K-1} |a_{k,n,m}|^2$ is the autocorrelation peak for the phase coding sequence on the nth subcarrier in the pulse transmitted by the mth element. The term $\boldsymbol{r}_{m,l}(n)$ is the nth element of the N-dimensional vector which is given by

$$\begin{aligned} \boldsymbol{r}_{m,l}(n) &= N\rho_l \exp[-\mathrm{j}2\pi(f_0 + \boldsymbol{\omega}(m)B_s)\tau_{m,l}] \cdot \exp[\mathrm{j}2\pi n\Delta f(p_0 - \tau_{m,l})] = \\ & N\rho_l \exp\{-\mathrm{j}2\pi[f_0 + (\boldsymbol{\omega}(m)N + n)\Delta f]\tau_{m,l}\} \cdot \exp(\mathrm{j}2\pi n\Delta f p_0) \end{aligned} \tag{23}$$

where the vector $\boldsymbol{\omega}$ is the carrier frequency coding sequence of M elements. For the last term in (16), the following relation holds:

$$\begin{aligned} \exp(\mathrm{j}2\pi n\Delta f p_0) &= \exp(\mathrm{j}2\pi\boldsymbol{\omega}(m)q)\exp(\mathrm{j}2\pi n\Delta f p_0) = \\ & \exp\left[\mathrm{j}2\pi\left(\boldsymbol{\omega}(m)q + n\Delta f\frac{qt_b}{N}\right)\right] = \\ & \exp\left\{\mathrm{j}2\pi(\boldsymbol{\omega}(m)N + n)\Delta f\frac{qt_b}{N}\right\} = \\ & \exp\{\mathrm{j}2\pi(\boldsymbol{\omega}(m)N + n)\Delta f p_0\}. \end{aligned} \tag{24}$$

Hence, the vector $\boldsymbol{r}_{m,l}(n)$ only depends on $(\boldsymbol{\omega}(m)N + n)$, plugging (24) into (23). The MN samples may be rearranged to be a vector according to the order of frequency values. A variable transform $\kappa = mN + n$ would enable the new vector to be represented by

$$\hat{\boldsymbol{r}}_l(\kappa) = N\rho_l \exp(-\mathrm{j}2\pi f_0 \tau'_{\kappa,l}) \exp[\mathrm{j}2\pi\kappa\Delta f(p_0 - \tau'_{\kappa,l})] \tag{25}$$

where $\tau'_{\kappa,l} = 2[R_{l0} + v\boldsymbol{\omega}^{-1}(m)T_{\mathrm{int}}]/c$ denotes the delay of the pulse where the κth frequency locates. Considering each element of the temporary vector $\boldsymbol{\omega}_{temp}(m)$ is the index which is used to explain where each argument of the sequence $[0, 1, 2, \cdots, M-1]$ is located in the vector $\boldsymbol{\omega}$. Each argument in the inverse frequency coding sequence $\boldsymbol{\omega}^{-1}$ is formed by repeating each element of $\boldsymbol{\omega}_{temp}$ for N times. For example, the transformation of $\boldsymbol{\omega}$ can be described as

$$\begin{aligned} \boldsymbol{\omega} &= [3 \quad 0 \quad 2 \quad 1] \rightarrow \boldsymbol{\omega}_{temp} = [1 \quad 3 \quad 2 \quad 0] \rightarrow \\ \boldsymbol{\omega}^{-1} &= [1 \cdot \boldsymbol{T}_{1,N} \quad 3 \cdot \boldsymbol{T}_{1,N} \quad 2 \cdot \boldsymbol{T}_{1,N} \quad 0 \cdot \boldsymbol{T}_{1,N}] \end{aligned} \tag{26}$$

where $\boldsymbol{T}_{1,N} = \underbrace{[1 \quad 1 \quad \cdots \quad 1]}_{N}$.

As can been seen in (25), the HRRP information of interest, the delay $\tau'_{\kappa,l}$, can be extracted by applying IDFT to the vector $\hat{\boldsymbol{r}}_l$ to reveal the scattering coefficients and positions of the scattering points. The IDFT result of the vector $\hat{\boldsymbol{r}}_l$ is expressed as

$$\begin{aligned}\boldsymbol{d}_l(l) = \sum_{\kappa=0}^{MN-1} \hat{r}_l(\kappa)\exp\left(\mathrm{j}2\pi\frac{\kappa l}{MN}\right) = \\ N\rho_l \exp(-\mathrm{j}2\pi f_0 \tau'_{\kappa,l})\cdot \\ \exp\left[\mathrm{j}\pi(MN-1)\left(\Delta f\Delta\tau_l + \frac{l}{MN}\right)\right]\cdot \\ \frac{\sin\left[\mathrm{j}\pi MN\left(\Delta f\Delta\tau_l + \frac{l}{MN}\right)\right]}{\sin\left[\mathrm{j}\pi\left(\Delta f\Delta\tau_l + \frac{l}{MN}\right)\right]}, \\ l = 0,1,2\dots,MN-1.\end{aligned} \tag{27}$$

where $\Delta\tau_l = p_0 - \tau'_{\kappa,l}$ and $\boldsymbol{d}_l$ is the HRRP of the target. When $\Delta f\Delta\tau_l + l/MN = \delta$ (δ is an arbitrary integer), the vector $|\boldsymbol{d}_l|$ comes to its peaks. Furthermore, the peak position can be described as

$$R_l = \frac{c}{2}\left[p_0 - \frac{1}{\Delta f}\left(\delta - \frac{l}{MN}\right)\right]. \tag{28}$$

As can be seen in (28), the range extent of the HRRP is derived from $c/(2\Delta f)$. It is noteworthy that all the peaks must locate in the same coarse range cell, i.e., $R_l \leqslant c/(2N\Delta f)$ such that the HRRP information can be retained completely.

The whole process is described in the flow diagram Fig. 4. The gain derives from the decoding and the IDFT processing marked as red boldface in the diagram. The first gain comes from the decoder, which is equal to K. The rest gain roots in the IDFT processing and is equal to MN, the number of all arguments in the vector $\boldsymbol{d}_l$. In a word, the signal-to-noise ratio (SNR) at the output should be $10\log(MNK)$ dB if additive white Gaussian noise adds up onto the echoes such that the SNR at the input is equal to 0 dB.

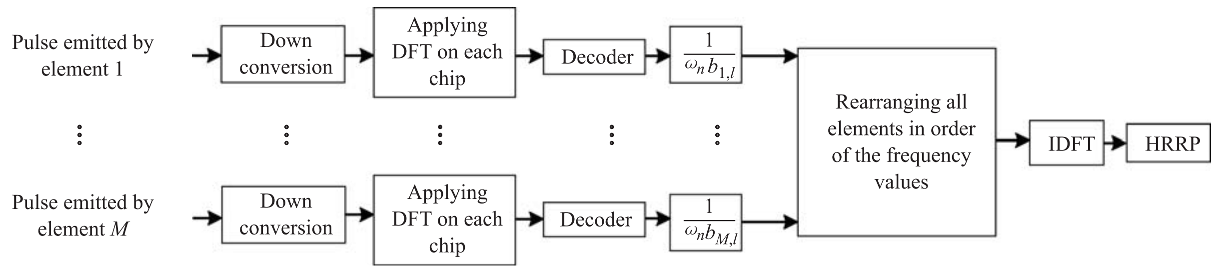

Fig. 4 Block diagram of the signal processing method

3. Velocity compensation for HRRP

In practice, the targets are usually on the move in most cases. The establishment of HRRP is fragile on account of motion of targets.

3.1 Scheme I

The scheme I presented in Fig. 2(a) explains that the echoes come from the pulses transmitted by all array elements simultaneously. Therefore, the translational radial velocity makes no difference to the pulses. The echo of the signal transmitted by the mth array element can be expressed by

$$\begin{aligned}s_{b,m}(t) = \sum_{l=1}^{L}\rho_l \exp(-\mathrm{j}2\pi f_m\tau_l)\cdot \\ \exp(\mathrm{j}2\pi f_{Dm,l}t)u_m(t-\tau_l)\end{aligned} \tag{29}$$

where $\tau_l = 2R_{l0}/c$, R_{l0} denotes the radial range of the lth scattering point. The difference between (4) and (29) is that the term $\exp(-\mathrm{j}2\pi f_m\tau_l)$ in (4) is not related to the velocity of the target at all. Assume that the intra-pulse Doppler can be neglected in this paper. The (29) can be simplified as

$$s_{b,m}(t) = \sum_{l=1}^{L}\rho_l \exp(-\mathrm{j}2\pi f_m\tau_l)u_m(t-\tau_l). \tag{30}$$

As a result, (25) may be expressed as

$$\hat{\boldsymbol{r}}_l(\kappa) = N\rho_l\exp(-\mathrm{j}2\pi f_0\tau'_{\kappa,l})\exp(\mathrm{j}2\pi\kappa\Delta f p_0). \tag{31}$$

Finally, the HRRP can be obtained after IDFT is applied to (31). For the suppression of the sidelobes, the Hanning window may be added before IDFT operation.

3.2 Scheme II

Scheme II is described in Fig. 2(b) vividly. The selected pulse of each array element has a PRI delay relative to the pulse transmitted by the prior element. The continuous and discrete forms of the echoes are as same as (4) and (18) respectively. The Doppler shift may induce the coarse range migration. The motion will further lead to the distortion of HRRP since the term $\exp(-\mathrm{j}2\pi f_m\tau_{m,l})$ disperses the energy of the peaks. Therefore, the terms related to velocity, $\exp(-\mathrm{j}2\pi f_0\tau'_{\kappa,l})$ and $\exp(\mathrm{j}2\pi\kappa\Delta f\tau'_{\kappa,l})$, are able to be compensated by the bank of filters constructed by the following vector

$$\begin{aligned}\boldsymbol{h}_c(\kappa) = \exp[\mathrm{j}2\pi f_0\boldsymbol{\omega}^{-1}(\kappa)T_{\mathrm{int}}\cdot 2v/c]\cdot \\ \exp[\mathrm{j}2\pi\kappa\Delta f\boldsymbol{\omega}^{-1}(\kappa)T_{\mathrm{int}}\cdot 2v/c].\end{aligned} \tag{32}$$

From another point of view, the filters can also act as an approach to estimate the velocity of the translational target.

4. Simulation and numerical analysis

In this section, a series of numerical analyses are performed to demonstrate the feasibility of the aforementioned schemes. Furthermore, the performance of resolving velocity ambiguity and suppressing noise is discussed. Scheme II is taken for an example to illustrate the superiority of the proposed methods here in consideration that Scheme II requires the velocity compensation but the Scheme I does not. To highlight the advantages of the proposed methods better, the simulation results based on the extended OFDM-MIMO will be compared with those of the OFD-LFM system discussed in [31]. The above radar systems with different transmitted waveforms are operated with the detail parameters listed in Table 1 and Table 2 respectively. Assume that a moving target has three scattering points which locate in [1 311 m, 1 314 m, 1 315.5 m], approaching the radar with translation velocity 161 m/s.

Table 1 OFD-LFM radar parameters

Parameter	Value
Carrier frequency/GHz	24
Bandwidth/MHz	20
Pulse width/μs	20
Pulse repetition interval/μs	50
Number of the array elements	50

Table 2 OFDM-MIMO radar parameters

Parameter	Value
Carrier frequency/GHz	24
Bandwidth of a single phase-coded OFDM symbol/MHz	20
Pulse width/μs	20
Pulse repetition interval/μs	50
Number of subcarriers	20
Subcarrier spacing/MHz	1
Number of chips	20
Number of the array elements	50

The performance of resolving velocity ambiguity is examined firstly. Assume that the SNR of the received echoes is 0 dB. For the OFD-LFM radar system, the difference between the adjacent coarse range cells is equal to $c/(2B_{cs})$ and B_{cs} is the frequency spacing. The OFD-LFM radar system utilizes a bank of FFT filters to estimate the velocity of the target while the coarse range cell is determined by using the stretch processing. The velocity detection range is from $-\lambda/(4 \cdot PRI)$ to $\lambda/(4 \cdot PRI)$, whereby the PRI determines the detection range without velocity ambiguity. As shown in Fig. 5, the velocity has been estimated correctly. In light of the above preparation, the estimated velocity is 161.13 m/s, and the coarse range cell is 1 290 m. The gap between the theoretical and measured values of the distance is caused by the range-Doppler coupling effect. Therefore, the HRRP can be presented in Fig. 6 after a necessary process: velocity compensation. For instance, the interpolation method in the frequency domain is a conventional method. However, when the PRI increases to 500 μs and other parameters do not change, the problem of velocity ambiguity occurs as shown in Fig. 7. In other words, the Doppler shift is forced to be folded since its frequency exceeds the measurement range. The wrong result of the velocity measurement which ignores velocity ambiguity is that the target is moving away from the radar at a speed of 139 m/s. Then the imaging must be wrong due to the wrong velocity compensation. Based on the proposed Scheme II, it can be seen clearly from Fig. 8 that the velocity is estimated correctly. The reason for the different results is that the detection range and accuracy of the proposed scheme depend on the bank of filters $\boldsymbol{h}_c(\kappa)$ and are irrelevant to the PRI. The comparison of velocity measurements illustrates that the proposed method has an outstanding performance of overcoming velocity ambiguity.

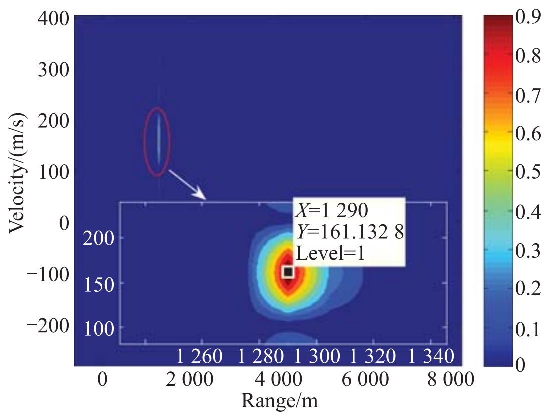

Fig. 5 Result of the velocity estimation using the OFD-LFM system

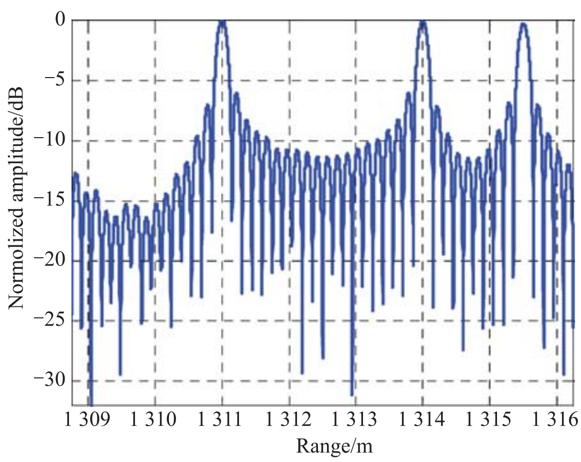

Fig. 6 Imaging result (4 096 points) of the OFD-LFM system

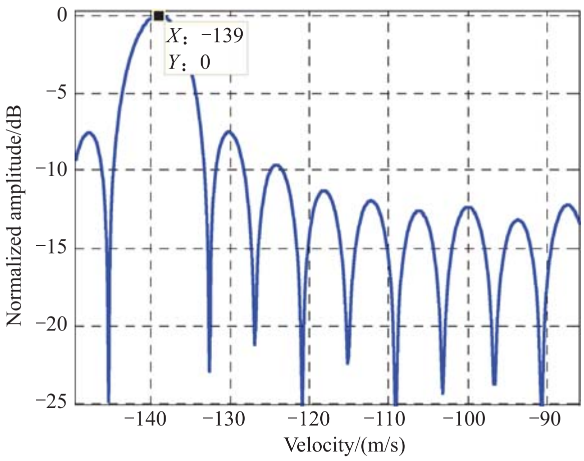

Fig. 7 Velocity estimation with velocity ambiguity in OFD-LFM system

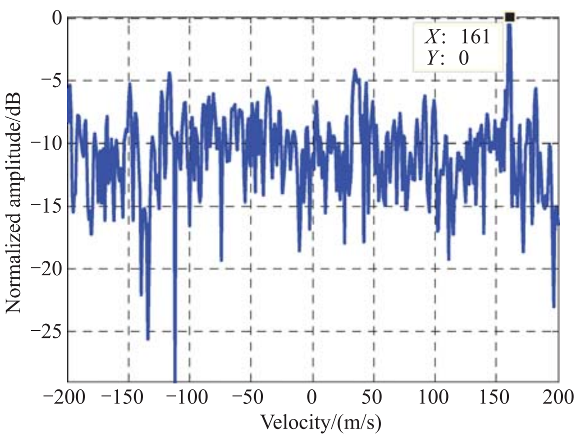

Fig. 8 Velocity estimation of the proposed method

Next, the performance of suppressing noise is investigated. The imaging experiments without velocity ambiguity are operated in the case of different SNRs. The imaging results can be obtained after the velocity compensation. Let the length of the HRRP be extended to 4 096 by zero-padding in the IDFT processing so as to improve the sampling resolution of the results. The imaging results achieved by the OFD-LFM system and extended OFDM-MIMO are compared in Fig. 9 where SNR is 0 dB. The pink line is acquired by the OFD-LFM system while the blue line and the red line are obtained by the proposed OFDM-MIMO system. As shown in Fig. 9, the maximum differences between the blue line and the pink line in the black ellipses are 12.46 dB and 10.62 dB respectively. The greatest difference value between the red line and the pink line is more than 20 dB. Namely, compared with the OFD-LFM system, the proposed method has a better performance of suppressing the correlation noise caused by the signal processing. This implies that the proposed scheme is able to make more power of the signal concentrate on the peaks than the OFD-LFM system, and the power of sidelobes is reduced. A further simulation has been carried out and depicted in Fig. 10, with the SNR decreasing to –20 dB. As shown in the enlarged view, the imaging result of the OFD-LFM system can hardly be recognized. However, both the HRRPs which are achieved by the proposed methods can be still identified. In detail, the imaging result in blue has an approximate 6.76 dB peak-to-sidelobe ratio. According to the red line, the peak-to-sidelobe ratio increases to around 12.73 dB after the Hanning window is applied. The performance of suppressing noise is improved by the proposed schemes due to orthogonality of the spectral components constituting the phase-coded OFDM signal.

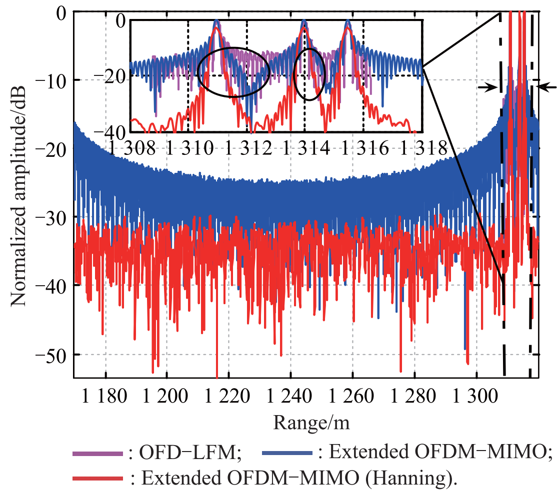

Fig. 9 Imaging results of the different methods (SNR = 0 dB)

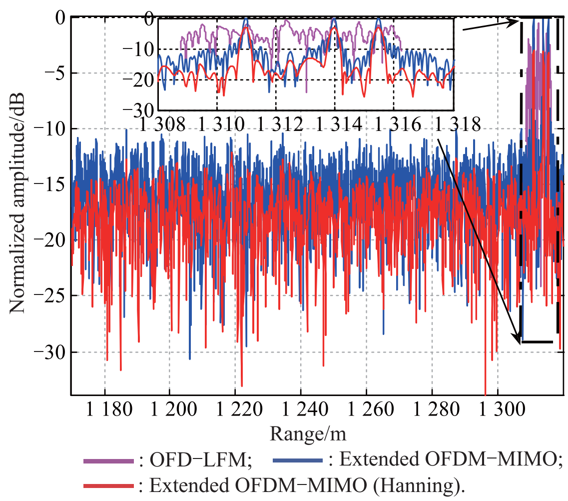

Fig. 10 Imaging results of the different methods (SNR = – 20 dB)

5. Benefits of the technology

In this section, the merits of the proposed schemes are summarized in light of the results produced by the proposed schemes and the OFD-LFM system. The advantages of the proposed schemes are listed as follows.

(i) In consideration of the low probability of detection characteristic, the phase-coded OFDM signal can be effective because the individual pulse appears like noise. As shown in Fig. 11, its power spectral density spreads in frequency domain, and its amplitude fluctuation is less than those of ordinary OFDM signals and chirp signals.

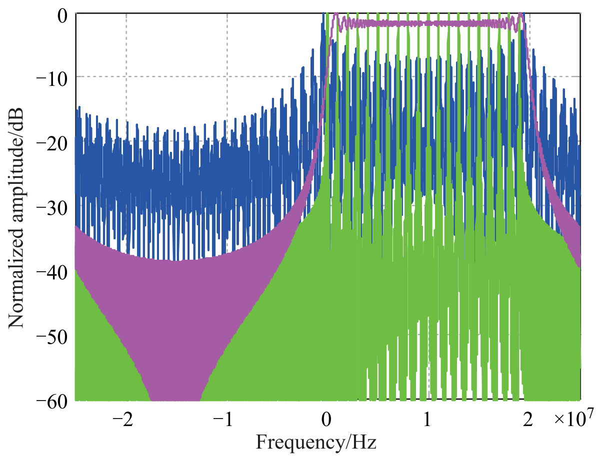

Fig. 11 Spectra of different signals with the same bandwidth

(ii) The velocity measurement scope of the proposed method overcomes the limitation of PRI as long as the scattering points of the target are located in the same coarse range cell. Furthermore, the measurement accuracy of velocity can be configured as required.

(iii) The range extent of HRRP produced by the proposed schemes is larger than that of the OFD-LFM system. The reason is that the range extent of the proposed methods is $c/(2\Delta f)$ which is determined by the frequency spacing of subcarriers, but that of the OFD-LFM system is equal to $c/(2B)$ which is related to the bandwidth of the single LFM pulse.

(iv) From the point of the view of suppressing noise, the attenuating speed and amplitude of the sidelobe level derived from the proposed schemes are much larger than those of the OFD-LFM system by comparison. Namely, the proposed method provides the mainlobes with more power than the OFD-LFM system. The orthogonality of the subcarriers constituting the phase-coded OFDM signal weakens the interaction effect between the spectral components in the signal processing. Therefore, the proposed schemes are effective in the case of low SNR.

(v) Currently, MIMO systems are gradually applied to both communication systems and radars. Our work is conducive to the progress of the joint radar and communication system.

6. Conclusions

In this paper, a new idea which exploits the phase-coded OFDM signal to generate the HRRP based on extended OFDM-MIMO is proposed. Our contributions are summarized as follows: (i) The phase-coded OFDM signal is applied to MIMO innovatively. (ii) The explicit comparisons of the velocity measurements and the imaging results made by the extended OFDM-MIMO and the existing OFD-LFM system are conducted, and the advantages of the proposed schemes are pointed out. (iii) The universal processing is given to obtain HRRP in the case of extended OFDM-MIMO radar with the random frequency coding. (iv) The proposed OFDM-MIMO platform can be utilized as a joint radar and communication platform in the future.

Considering the future study, it is worth mentioning that finding a set of modulation sequences for subcarriers to suppress the peak-to-average-power ratio is important. Moreover, the effect of the phase coding on the phase-coded OFDM signal should be analyzed. Another future work ought to concentrate on the performance analysis of the processing in multiple scattering points with different radial velocities.

References

[1] M. Uchida, Y. Kagawa, A. Okuno. A vehicle-to-vehicle communication and ranging system based on spread spectrum technique-SS communication radar. *Proc. of the Vehicle Navigation and Information Systems Conference*, 1994: 169 – 174.

[2] G. Lellouch, H. Nikookar. On the capability of a radar network to support communications. *Proc. of the IEEE Symposium on Communications & Vehicular Technology*, 2007: 1 – 5.

[3] B. C. Flores. Fourier transform receiver processing of hopped frequency sequences for synthetic range profile generation. *SPIE - Radar Processing, Technology, and Applications*, 1996, 2845: 14 – 25.

[4] N. Levanon. Stepped-frequency pulse-train radar signal. *IEE Radar, Sonar and Navigation*, 2002, 149(6): 297 – 309.

[5] D. E. Maron. Frequency-jumped burst waveforms with stretch processing. *Proc. of the IEEE International Radar Conference*, 1990: 274 – 279.

[6] H. Schimpf, A. Wahlen, Essen H. High range resolution by means of synthetic bandwidth generated by frequency-stepped chirps. *Electronics Letters*, 2003, 39(18): 1346 – 1348.

[7] W. K. Gu, D. W. Wang, X. Y. Ma. High speed moving target detection using distributed OFDM-MIMO phased radar. *Proc. of the 12th International Conference on Signal Processing*, 2014: 2087 – 2091.

[8] W. K. Gu, D. W. Wang, X. Y. Ma, et al. Incoherent integration detection using distributed OFDM-MIMO radar. *Systems Engineering and Electronics*, 2015, 37(10): 2266 – 2271. (in Chinese)

[9] W. Q. Wang. Large time-bandwidth product MIMO radar waveform design based on chirp rate Diversity. *IEEE Sensors Journal*, 2015, 15(2): 1027 – 1034.

[10] IEEE. IEEE Standard for Information Technology - Telecommunications and Information Exchange Between Systems - Local and Metropolitan Area Networks - Specific Requirements. Part 11: Wireless LAN Medium Access Control (MAC) and Physical Layer, 2003: 0_1 – 121.

[11] L. Dai, Z. Wang, Z. Yang. Time-frequency training OFDM with high spectral efficiency and reliable performance in high speed environments. *IEEE Journal on Selected Areas in Communications*, 2012, 30(4): 695 – 707.

[12] R. F. Tigrek, W. J. A. De Heij, P. Van Genderen. OFDM signals as the radar waveform to solve Doppler ambiguity. *IEEE Trans. on Aerospace & Electronic Systems*, 2012, 48(48): 130 – 143.

[13] C. Sturm, W. Wiesbeck. Waveform design and signal processing aspects for fusion of wireless communications and radar sensing. *Proceedings of the IEEE*, 2011, 99(7): 1236 – 1259.

[14] G. Lellouch, A. Mishra, M. Inggs. Impact of the Doppler modulation on the range and Doppler processing in OFDM radar. *Proc. of the IEEE Radar Conference*, 2014: 803 – 808.

[15] G. Lellouch, P. Tran, R. Pribic, et al. OFDM waveforms for frequency agility and opportunities for Doppler processing in radar. *Proc. of the IEEE Radar Conference*, 2008: 1 – 6.

[16] G. Lellouch, R. Pribic, P. Van Genderen. Frequency agile stepped OFDM waveform for HRR. *Proc. of the International Waveform Diversity and Design Conference*, 2009: 90 – 93.

[17] K. Huo, B. Deng, Y. Liu, et al. The principle of synthesizing HRRP based on a new OFDM phase-coded stepped-frequency radar signal. *Proc. of the IEEE International Conference on Signal Processing*, 2010: 1994 – 1998.

[18] K. Huo, B. Deng, Y. Liu, et al. High-resolution range profile analysis based on multicarrier phase-coded waveforms of OFDM radar. *Journal of Systems Engineering and Electronics*, 2011, 22(3): 421 – 427.

[19] G. Lellouch, A. K. Mishra, M. Inggs. Stepped OFDM radar technique to resolve range and Doppler simultaneously. *IEEE Trans. on Aerospace & Electronic Systems*, 2015, 51(2): 937 – 950.

[20] F. Q. Wen, G. Zhang, D. Ben. Direction-of-arrival estimation for co-located multiple-input multiple-output radar using structural sparsity Bayesian learning. *Chinese Physics B*, 2015, 24(11): 70 – 76.

[21] F. Q. Wen, G. Zhang. Multi-way compressive sensing based 2D DOA estimation algorithm for monostatic MIMO radar with arbitrary arrays. *Wireless Personal Communications*, 2015, 85(4): 2393 – 2406.

[22] H. J. Wang. Study on MIMO radar imaging based on antenna array. *Signal Processing*, 2009, 25(8): 1203 – 1208.

[23] Y. T. Zhu, W. X. Yu, S. U. Yi. An ISAR imaging method based on MIMO technique. *IEEE Trans. on Geoscience & Remote Sensing*, 2010, 48(8): 3290 – 3299.

[24] D. W. Wang, X. Y. Ma, A. L. Chen, et al. High-resolution imaging using a wideband MIMO radar system with two distributed arrays. *IEEE Trans. on Image Processing*, 2010, 19(5): 1280 – 1289.

[25] H. J. Wang, H. B. Xu, L. U. Min, et al. High-resolution imaging method based on MIMO radar. *Journal of Microwaves*, 2009, 25(5): 79 – 83.

[26] X. Z. Dai. High resolution range imaging and sidelobe suppression based on FD-MIMO radar. *Journal of Electronics and Information Technology*, 2008, 30(9): 2033 – 2037.

[27] C. Gu. Signal processing and detecting for multicarrier modulated radar system based on OFDM. *Journal of Electronics and Information Technology*, 2009, 31(6): 1298 – 1300.

[28] M. L. Yang. A novel signal processing approach for the multicarrier MIMO radar. *Journal of Electronics and Information Technology*, 2009, 31(1): 147 – 151.

[29] B. Liu, C. L. Han, J. H. Miao. OFD-LFM signal design and performance analysis for MIMO radar. *Journal of University of Electronic Science & Technology of China*, 2009, 39(5): 688 – 691.

[30] L. Ying. Micro-Doppler effect analysis of rotating target and three-dimensional micro-motion feature extraction in OFD-LFM MIMO radar. *Journal of Electronics and Information Technology*, 2011, 33(1): 8 – 13.

[31] X. H. Huang, X. J. Li. Moving target HRRP synthesizing-method for MIMO radar with OFD-LFM signal. *Journal of Air Force Engineering University*, 2012, 12(5): 30 – 34.

[32] B. J. Donnet, I. D. Longstaff. Combining MIMO radar with OFDM Communications. *Proc. of the Radar Conference*, 2006: 37 – 40.

Biographies

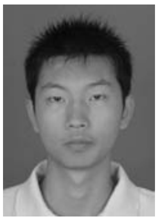

Xinhai Wang was born in 1988. He received his B.S. degree in School of Electronic Information Engineering from Nanjing University of Information Science & Technology, Nanjing, China, 2012, and his M.S. degree in College of Electronics and Information Engineering, Nanjing University of Aeronautics and Astronautics (NUAA), 2014. He is a Ph.D. candidate in College of Electronics and Information Engineering, NUAA. His research interests are array signal processing, wireless communication, and signal processing.
E-mail: wangxinhai@nuaa.edu.cn

Gong Zhang was born in 1964. He received his Ph.D. degree in electronic engineering from Nanjing University of Aeronautics and Astronautics (NUAA), Nanjing, China, in 2002. Since 1998, he has been with the College of Electronic and Information Engineering, NUAA, where he is currently a professor. He is a member of Committee of Electromagnetic Information, Chinese Society of Astronautics (CEI-CSA) and a senior member of the Chinese Institute of Electronics (CIE). His research interests are radar signal processing and classification recognition.
E-mail: gzhang@nuaa.edu.cn

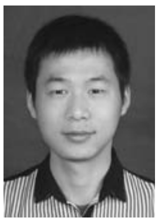

Fangqing Wen was born in 1988. He received his B.S. degree in electronic engineering from Hubei University of Automotive Technology, Shiyan, China, 2011. From 2011 to 2016, he was pursuing his Ph.D. degree in College of Electronics and Information Engineering, Nanjing University of Aeronautics and Astronautics (NUAA). Now he is lecturer in Electronic and Information School, Yangtze University. His research interests are compressive sensing, wireless communication and signal processing.
E-mail: wfqltt@163.com

De Ben was born in 1938. He received his B.S. degree of radar from Harbin Institute of Technology, Harbin, China, in 1963. In 1963, he joined the Nanjing Research Institute of Electronics Technology. In 2001, he became an Academician of China Engineering Academy. He is an expert in radar system, and he is a member of the Chinese Institute of Electronics (CIE). He is currently a professor in Nanjing University of Aeronautics and Astronautics (NUAA). His current research interests include radar network, radar detection and radar system.
E-mail: bende01@sohu.com